JMEPEG (2008) 17:168–177
DOI: 10.1007/s11665-007-9179-z

1059-9495/$19.00

Analytical Modeling of Strain Rate Distribution During Friction Stir Processing

B.M. Darras and M.K. Khraisheh

(Submitted September 19, 2007)

Friction Stir Processing (FSP) is becoming an acceptable technique for modifying the grain structure of sheet metals. One of the most important issues that hinder the widespread use of FSP is the lack of accurate models that can predict the resulting microstructure in terms of process parameters. Most of the work that has been done in the FSP field is experimental, and limited modeling activities have been conducted. In this work, an analytical model is presented that can predict the strain rate distribution and the deformation zone in the friction stir processed zone as a function of process parameters. In the model, the velocity fields within the processed zone are determined by incorporating the effects of both the shoulder and the pin of the tool on the material flow. This is achieved by introducing state variables and weight functions. The model also accounts for different interfacial conditions between the tool and the material. The effects of different process parameters and conditions on the velocity fields and strain rate distributions are discussed. The results clearly show that the model can successfully predict the shape of the deformation zone and that the predicted strain rate values are in good agreement with results reported in the literature.

Keywords friction stir processing, interfacial contact conditions, microstructure modification, severe plastic deformation, strain rate distribution

1. Introduction

Aluminum welding has always been a great challenge, which motivated the researchers at TWI to invent a new advanced welding technique, friction stir welding (FSW) (Ref 1). It was observed that the welding zone is characterized by equiaxed fine grain structure. As a result, the concept of FSW was extended to a new advanced microstructural modification process in the late 1990s, Friction Stir Processing (FSP). Since then, many researchers have investigated several aspects of the process. It has been reported that FSP can enhance the superplasticity of lightweight materials through producing an equiaxed ultrafine grain structure and favorably modifying the material properties (Ref 2-5). During FSP, a specially designed rotating tool which consists of a pin and a shoulder is used. The rotating pin is plunged into the sheet, traversing in the desired direction, while the shoulder is rubbing against the surface of the sheet generating enough heat (remains solid state) to soften the material beneath the tool. The mechanical stirring caused by the plunged rotating pin forces the softened material to undergo intense plastic deformation yielding a processed zone

This article was presented at the AeroMat Conference, International Symposium on Superplasticity and Superplastic Forming (SPF) held in Baltimore, MD, June 25-28, 2007.

B.M. Darras and **M.K. Khraisheh**, Center for Manufacturing and Department of Mechanical Engineering, University of Kentucky, Lexington, KY 40506. Contact e-mail: Khraisheh@engr.uky.edu.

Nomenclature

r	Radial distance from the tool center (m)
r_p	Pin radius (m)
r_s	Shoulder radius (m)
z	Distance from top to bottom in the thickness direction (m)
z_o	Pin height (m)
θ	The angle from the radial axis at the middle section of the tool (moving clockwise when looking from the top) (radians)
ω	Rotational speed of the tool (rad/s)
v	Translational speed of the tool (m/s)
$V_{material}$	FS-processed material resultant velocity (m/s)
$V_{shoulder}$	Shoulder resultant velocity (m/s)
V_{pin}	Pin resultant velocity (m/s)
η	Material/pin state variable
λ	Material/shoulder state variable
$u_{(s)\theta}$	Material velocity component caused by shoulder in the θ direction (m/s)
$u_{(s)r}$	Material velocity component caused by shoulder in the r direction (m/s)
$u_{(p)\theta}$	Material velocity component caused by pin in the θ direction (m/s)
$u_{(p)r}$	Material velocity component caused by pin in the r direction (m/s)
$w_{(s)\theta}$	Shoulder weight function in the θ direction
$w_{(s)r}$	Shoulder weight function in the r direction
$w_{(p)\theta}$	Pin weight function in the θ direction
$w_{(p)r}$	Pin weight function in the r direction
u_θ	Material resultant velocity component in the θ direction (m/s)
u_r	Material resultant velocity component in the r direction (m/s)
u_z	Material resultant velocity component in the z direction (m/s)
$\dot{\varepsilon}_{eff}$	Effective strain rate (1/s)

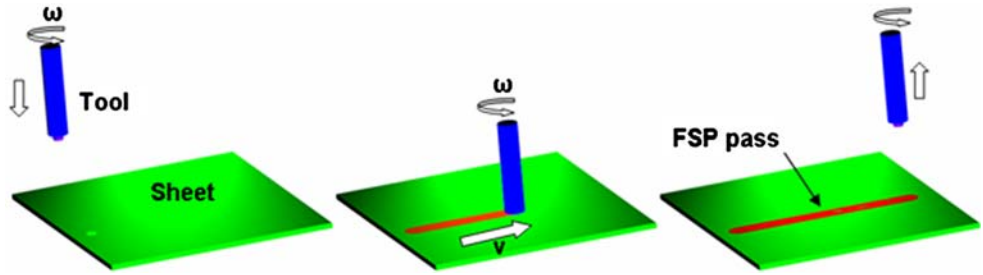

Fig. 1 Schematic of FSP

characterized by dynamically recrystallized fine grain structure. Figure 1 shows a schematic of FSP.

In order to advance the utilization of FSP in sheet metal processing and fabrication, accurate models are needed to enable process simulation and optimization. Most of the modeling discussed in the literature focuses on the thermal aspect of the process and limited work consider both thermal and mechanical features.

Ulysse (Ref 6) proposed a 3D viscoplastic model for FSW to determine the effect of tool speed on temperature. Chang et al. (Ref 7) attempted to develop a relation between grain size and Zener-Holloman parameter for friction stir-processed AZ31 Mg alloy. Heurtier et al. (Ref 8) proposed a thermomechanical analysis of FSW, in which a model for material flow pattern was proposed. They divided the weld zone into two and used classical fluid mechanics to determine the velocity fields assuming incompressible and kinematically admissible flow. Schmidt et al. (Ref 9) proposed an analytical model for heat generation in FSW and studied different contact conditions between the tool and the weld; sliding, sticking, and partial sliding/sticking. Arbegast (Ref 10) proposed a simple model based on metalworking processes and presented relationships to calculate the extrusion zone width, strain rate, and pressure. Schneider and Nunes (Ref 11) described in their mathematical model the material flow path in friction stir welds and proposed three incompressible flow fields that together describe the material flow in friction stir welds. Nandan et al. (Ref 12) solved the equations of conservation of mass, momentum, and energy numerically and computed the spatial variation of the non-Newtonian viscosity. Buffa et al. (Ref 13) used a Finite Element model, which was calibrated experimentally, to investigate the temperature and strain distributions.

Although it is agreed that the temperature and strain rate distributions in the processed zone are the main factors that control the resulting grain structure, there exists no clear and accurate model to estimate the strain rate distribution within the FSP zone in terms of process parameters and ultimately relate the resulting microstructure to process parameters.

The current work presents a model that estimates the strain rate distribution within the friction stir-processed zone in terms of process parameters. In this model, the velocity fields within the processed zone are determined by considering the effects of both the shoulder and the pin of the tool on the material flow. State variables are introduced to relate the material velocity in the processed zone to the velocity of the tool (the shoulder and the pin). In addition, weight functions are introduced to determine the contribution of the shoulder and the pin on the material flow within the processed zone. From the velocity fields, the strain rate distribution in the processed zone can then be estimated. Different scenarios are considered to investigate the effects of both the pin and the shoulder on the material flow and consequently on the strain rate distribution. The effects of contact conditions at the tool/sheet interfaces and process parameters (rotational and translational speeds) are also investigated.

2. Model Development

The ultimate goal is to develop a physics-based model that can accurately predict the resulting microstructure of FS-processed material in terms of process parameters. The model presented below serves as a first step toward that goal in order to enable FSP to "design" a certain microstructure for optimum performance.

FSP is considered as a hot working process where the flow stress is highly dependent on temperature and the stain rate. The resulting grain structure in the processed zone mainly depends on the resulting strain rate and temperature distributions. In order to be able to achieve a desired microstructure, the strain rate and temperature distributions must be controlled and related to the grain structure and process parameters.

This work attempts to develop an analytical model to predict the strain rate distribution during FSP. The framework of this model is as follows:

- State variables that relate the material velocity to the tool velocity (shoulder and pin) are first introduced.
- Weight functions are also introduced to determine how much the tool shoulder and the tool pin contribute to the net flow of material in the processed zone.
- The velocity fields in the processed zone are then determined as a function of process parameters.
- Finally, the strain rate distribution in the deformed (processed) zone is calculated from the velocity fields.

For convenience, a table of nomenclature is included for easy reference to the different terms and symbols used in the following equations. A schematic of the proposed model is shown in Fig. 2 illustrating the tool/sheet interfaces and the proposed geometry of the deformation zone. In this work, the dimensions of the radii of the pin and the shoulder are r_p = 3.175 mm and r_s = 6.350 mm, respectively. These numbers are the actual dimensions of the tool currently used in our laboratory to conduct FSP experiments (Ref 4, 5, 14). A flat shoulder and a flat cylindrical pin are considered in this analysis. The sheet thickness is z_o = 3.175 mm (see Fig. 2). In this work,

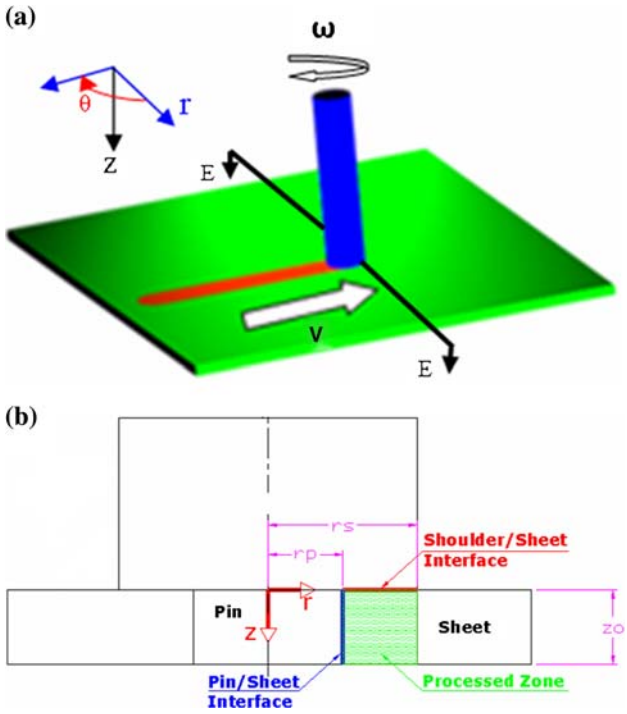

Fig. 2 Model's geometry: (a) 3D and (b) cross section EE

different rotational speeds (400-600 rpm) and translational speeds (0.847-2.540 mm/s) are covered. These values are typical of speeds used in FSP of aluminum alloys (Ref 2, 4, 14).

The main assumptions that have been made for developing the model include:

- Two incompressible flow fields are combined to describe the material flow: rigid body rotation and uniform translation.
- No material movement in the thickness direction is considered.
- The contact condition is constant along each interface; however, different contact conditions can be used.
- The overall velocity field in the processed zone is determined by combining the velocity fields based on the movements of the tool shoulder and the tool pin independently using weight functions.

2.1 State Variables

The first step is to define how the material velocity is related to the tool velocity. There are several factors that control this relation including contact condition at the tool/sheet interfaces, tool geometry, sheet clamping force, material properties, temperature, and pressure. In order to consider these effects, state variables are introduced. There are two interfaces between the tool and the sheet: one is at the shoulder and the other is at the pin (as shown in Fig. 2). The material flow and movement is influenced by both the shoulder and the pin in different ways; the shoulder is mainly responsible for material flow near the sheet surface while the pin is responsible for stirring the material through the sheet thickness. For this reason, two state variables are needed. The first one is denoted η (see Eq 1-2), which relates the material velocity to the shoulder velocity, and it is defined as a function of z (the distance from top to bottom in the thickness direction). Two other parameters are used to define η; the first one is A which represents the contact state at the shoulder/material interface. The value of A varies between 0 and 1; 1 for full sticking, 0 for full slipping and $0 < A < 1$ for combined sticking-slipping contact condition. The second parameter used to define η is B which accounts for the effect of material properties, temperature, and pressure. The same approach is followed to define the second state variable λ (see Eq 3-4), which relates the material velocity to the pin velocity. The state variable λ is defined in terms of r (the radial distance from the tool center), and the two parameters C and D (C is equivalent to A and D is equivalent to B). Mathematically, the state variables are given by:

$$\eta = \frac{V_{\text{material}}}{V_{\text{Shoulder}}} \quad \text{(Eq 1)}$$

$$\eta = A \exp\left(-B\frac{z}{z_{\text{o}}}\right) \quad \text{(Eq 2)}$$

$$\lambda = \frac{V_{\text{material}}}{V_{\text{pin}}} \quad \text{(Eq 3)}$$

$$\lambda = C \exp\left(-D\frac{(r - r_{\text{p}})}{(r_{\text{s}} - r_{\text{p}})}\right) \quad \text{(Eq 4)}$$

To explain the physical meaning of these state variables, consider the state variable, η relating the material velocity resulting from the shoulder movement to the shoulder velocity. At the sheet surface ($z = 0$), the state variable (η) equals the parameter A. For full sticking condition, A equals 1, which result in a material velocity equals to the shoulder velocity. For full slipping condition ($A = 0$), the material is stagnant at the sheet surface. The physical meaning of the state variable relating the material velocity resulting from the pin movement to the pin velocity is analogous to the one described above.

2.2 Weight Functions

The shoulder and the pin both affect the material movement within the processed zone. To account for how much each of them is responsible for the material flow, weight functions are introduced. The main idea is to assume as if the two act independently and then combine their effect. First, it is assumed that the shoulder is only responsible for the material flow (and no material movement is resulted from the pin) and the velocity field from this scenario is determined. Second, the velocity field is determined assuming the material movement and the flow is only caused by the pin. Finally, the two velocity fields are combined using the weight functions to yield the overall velocity field. The weight functions for the shoulder and the pin are defined in both r and θ coordinates (θ is the angle from the radial axis at the middle section of the tool as shown in Fig. 2a) as given below in Eq 5-8.

$$w_{(\text{s})\theta} = \frac{u_{(\text{s})\theta}}{u_{(\text{s})\theta} + u_{(\text{p})\theta}} \quad \text{(Eq 5)}$$

$$w_{(\text{p})\theta} = \frac{u_{(\text{p})\theta}}{u_{(\text{s})\theta} + u_{(\text{p})\theta}} \quad \text{(Eq 6)}$$

$$w_{(\text{s})r} = \frac{u_{(\text{s})r}}{u_{(\text{s})r} + u_{(\text{p})r}} \quad \text{(Eq 7)}$$

$$w_{(p)r} = \frac{u_{(p)r}}{u_{(s)r} + u_{(p)r}} \quad \text{(Eq 8)}$$

2.3 Velocity Fields

Two incompressible flow fields are combined to describe the material flow in the FS-processed zone: rigid body rotation and uniform translation. The material movement in the z direction is not considered in this analysis. The velocities of both the shoulder and the pin are described in terms of the rotational and translational speeds of the tool along with the state variables (Eq 9-12):

$$u_{(s)\theta} = \eta[\omega r - v\cos(\theta)] \quad \text{(Eq 9)}$$

$$u_{(s)r} = \eta[-v\sin(\theta)] \quad \text{(Eq 10)}$$

$$u_{(p)\theta} = \lambda[\omega r_p - v\cos(\theta)] \quad \text{(Eq 11)}$$

$$u_{(p)r} = \lambda[-v\sin(\theta)] \quad \text{(Eq 12)}$$

Incorporating the weight functions with these velocity fields yields the overall velocity field in the r-θ-z coordinates as given by Eq 13-15.

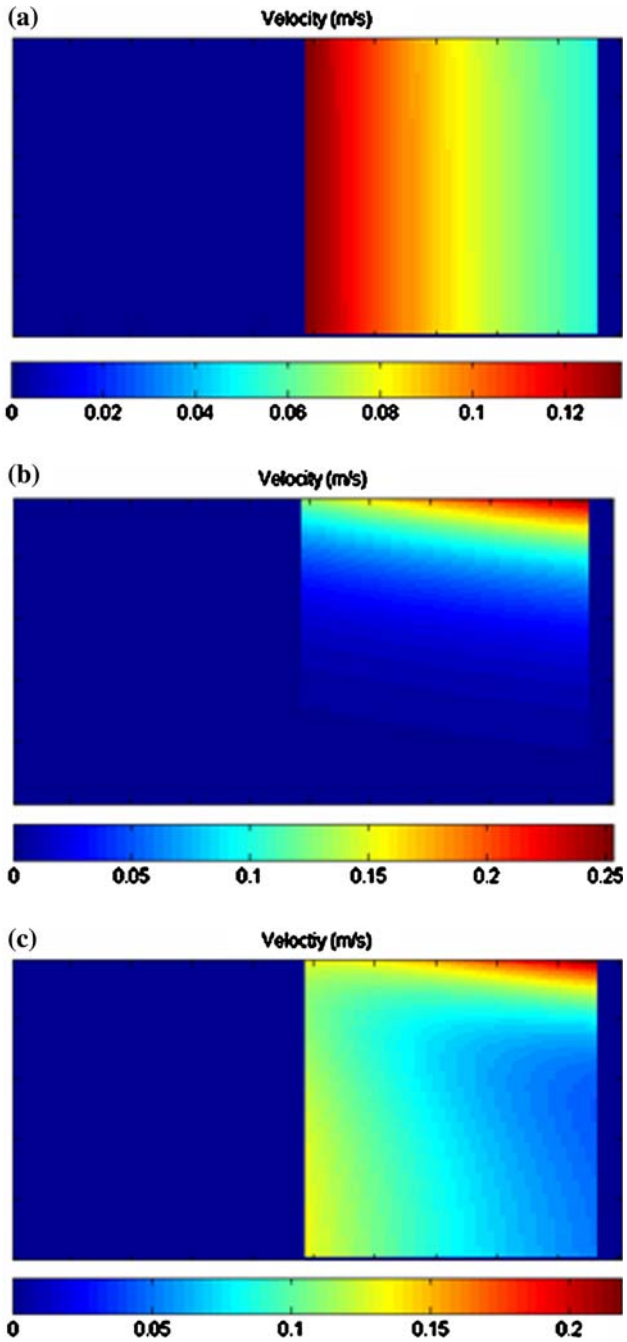

Fig. 3 Velocity fields for FSP at 400 rpm and 0.847 mm/s: (a) pin alone, (b) shoulder alone, and (c) combined shoulder and pin

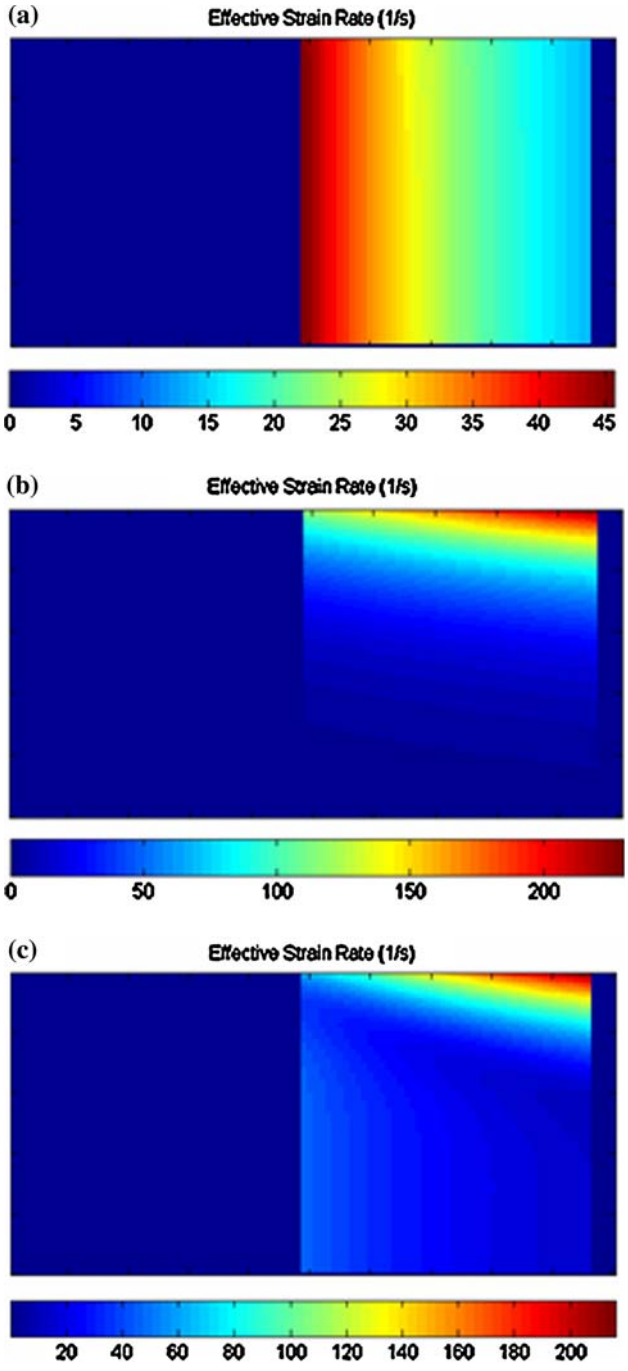

Fig. 4 Strain rate distributions for FSP at 400 rpm and 0.847 mm/s: (a) pin alone, (b) shoulder alone, and (c) combined shoulder and pin

$$u_\theta = w_{(s)\theta} u_{(s)\theta} + w_{(p)\theta} u_{(p)\theta} \quad \text{(Eq 13)}$$

$$u_r = w_{(s)r} u_{(s)r} + w_{(p)r} u_{(p)r} \quad \text{(Eq 14)}$$

$$u_z = 0 \quad \text{(Eq 15)}$$

2.4 Strain Rate

The velocity-strain rate relations in cylindrical coordinate are used to find the strain rate components (equations' set 16) (Ref 15). The effective strain rate distribution within the FS-processed zone can be determined assuming von Mises according to Eq 16.

$$\left\{ \begin{array}{l} \dot{\varepsilon}_{rr} = \frac{\partial u_r}{\partial r} \\ \dot{\varepsilon}_{\theta\theta} = \frac{1}{r}\frac{\partial u_\theta}{\partial \theta} - \frac{u_r}{\partial r} \\ \dot{\varepsilon}_{zz} = \frac{\partial u_z}{\partial z} \\ \dot{\varepsilon}_{r\theta} = \frac{1}{2}\left[\frac{1}{r}\frac{\partial u_r}{\partial \theta} + \frac{\partial u_\theta}{\partial r} - \frac{u_\theta}{r}\right] \\ \dot{\varepsilon}_{\theta z} = \frac{1}{2}\left[\frac{\partial u_\theta}{\partial z} + \frac{1}{r}\frac{\partial u_z}{\partial \theta}\right] \\ \dot{\varepsilon}_{zr} = \frac{1}{2}\left[\frac{\partial u_z}{\partial r} + \frac{\partial u_r}{\partial z}\right] \end{array} \right\} \quad \text{(Eq 16)}$$

$$\dot{\varepsilon}_{\text{eff}} = \left(\frac{2}{3}\dot{\varepsilon}_{ij}{}^2\right)^{1/2} \quad \text{(Eq 17)}$$

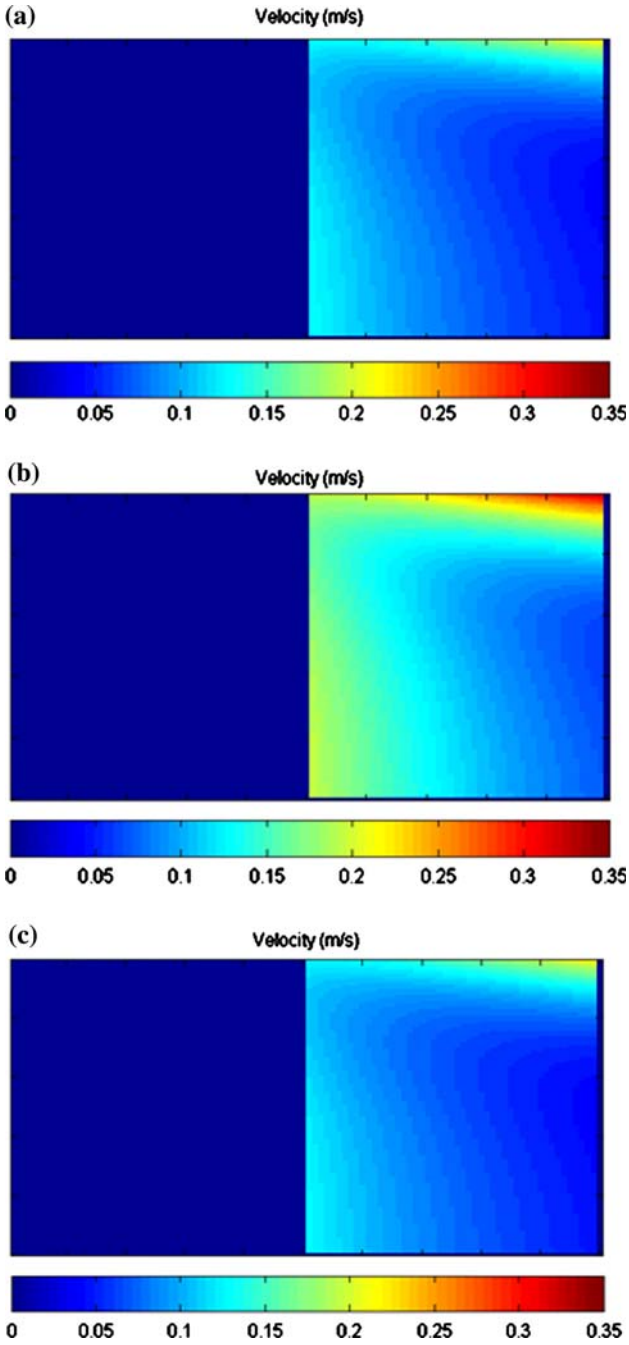

Fig. 5 Velocity field for FSP at (a) 400 rpm and 0.847 mm/s, (b) 600 rpm and 0.847 mm/s, (c) 400 rpm and 2.540 mm/s

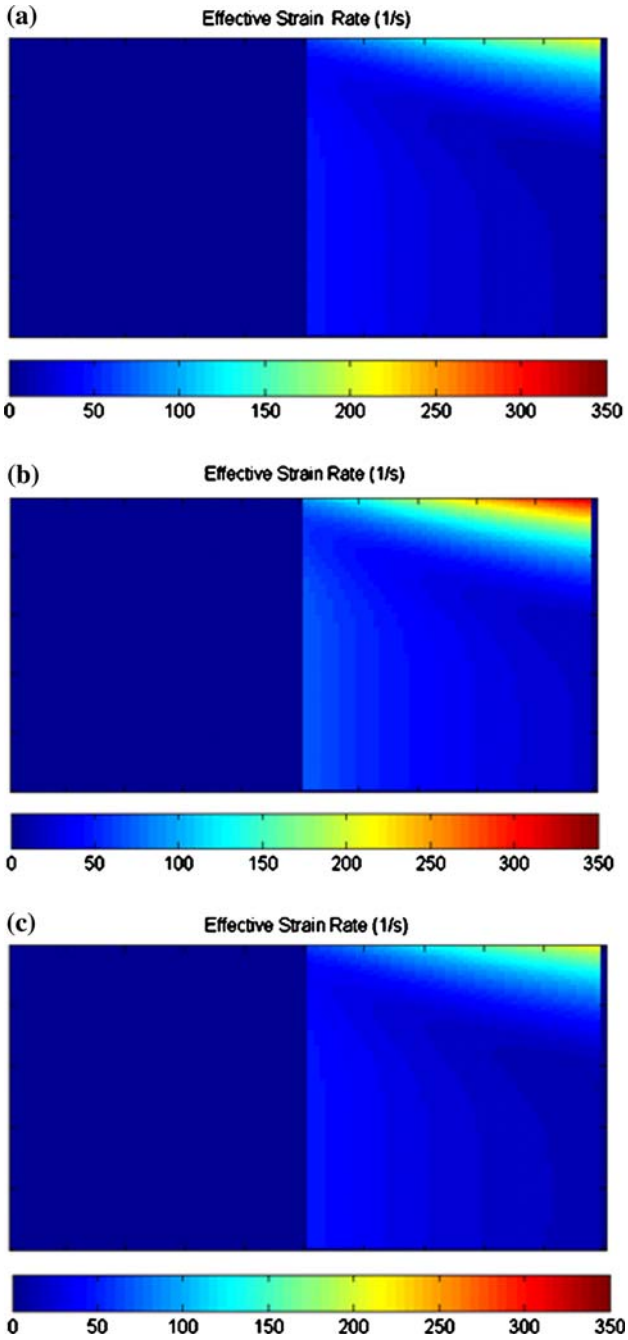

Fig. 6 Strain rate distributions for FSP at (a) 400 rpm and 0.847 mm/s, (b) 600 rpm and 0.847 mm/s, and (c) 400 rpm and 2.540 mm/s

3. Results and Discussion

3.1 Shoulder and Pin Effects

The effects of the shoulder and the pin, separately and combined, on material deformation within the FS-processed zone are illustrated by the three velocity fields shown in Fig. 3. It is obvious that when considering the effect of the pin alone (Fig. 3a), the material velocity decreases as the radial distance from the tool's center increases, as illustrated by Eq 4 and 11. It is important to note that the velocity at a given radius is constant along the thickness (z) direction because the velocity depends on the radius and the contact condition at the pin/material interface. In this analysis, it is assumed that the contact condition does not change along the pin/material interface. Considering the shoulder effect (Fig. 3b), the results show that the material velocity increases as the radial distance from the tool's center increases and the distance along the thickness from

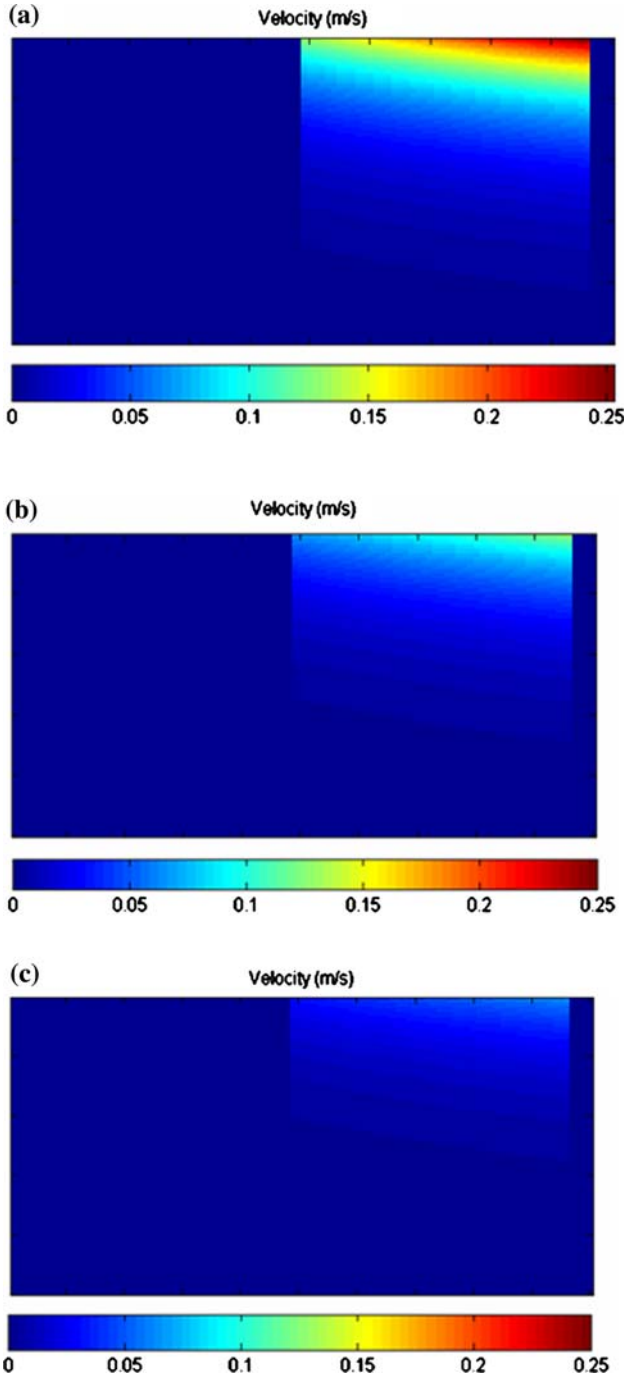

Fig. 7 Velocity field for separate shoulder effect scenario (FSP at 400 rpm and 0.847 mm/s): (a) full sticking at the shoulder/sheet interface (A = 1.0), (b) 50% sticking at the shoulder/sheet interface (A = 0.5), and (c) 25% sticking at the shoulder/sheet interface (A = 0.25)

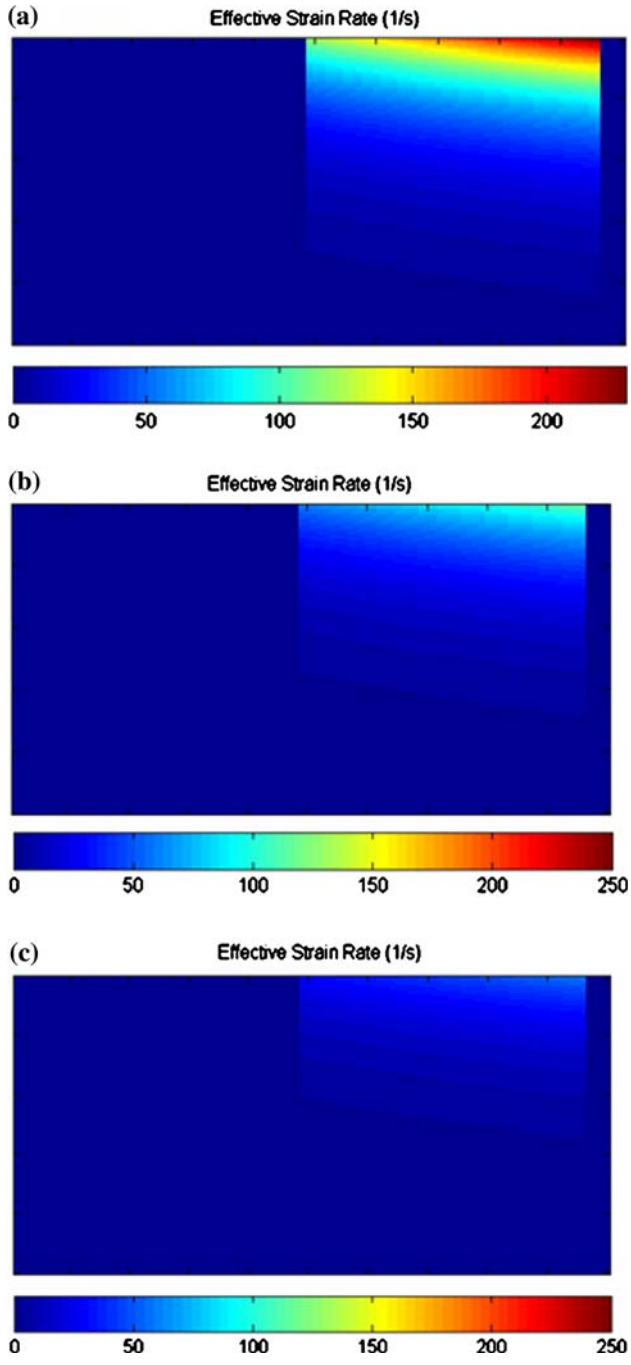

Fig. 8 Strain rate distribution for separate shoulder effect scenario (FSP at 400 rpm and 0.847 mm/s): (a) full sticking at the shoulder/sheet interface (A = 1.0), (b) 50% at the shoulder/sheet interface sticking (A = 0.5), and (c) 25% sticking at the shoulder/sheet interface (A = 0.25)

the top surface of the sheet decreases as illustrated by Eq 2 and 9. Figure 3(c) shows the combined effects of the shoulder and the pin on the material velocity. The maximum velocity occurs at the outer edge of the shoulder/sheet interface in agreement with the findings of Nandan et al. (Ref 12). Similar trends are noticed for the strain rate distributions, as shown in Fig. 4. It is very important to note that the obtained strain rate values are in the order of hundreds, which are in agreement with reported values in the literature (Ref 9, 12). Schmidt et al. (Ref 9) showed in their work that the shear rate was in the order of hundreds, and Nandan et al. (Ref 12) predicted the maximum strain rate to be about 160 s^{-1}. The high strain rate values confirm that intense plastic deformation at high rates is taking place during FSP.

3.2 Rotational and Translational Speeds Effects

The effects of the rotational and translational speeds on the velocity fields and strain rate distributions are shown in Fig. 5 and 6. As shown in the figures, the velocity and strain rate

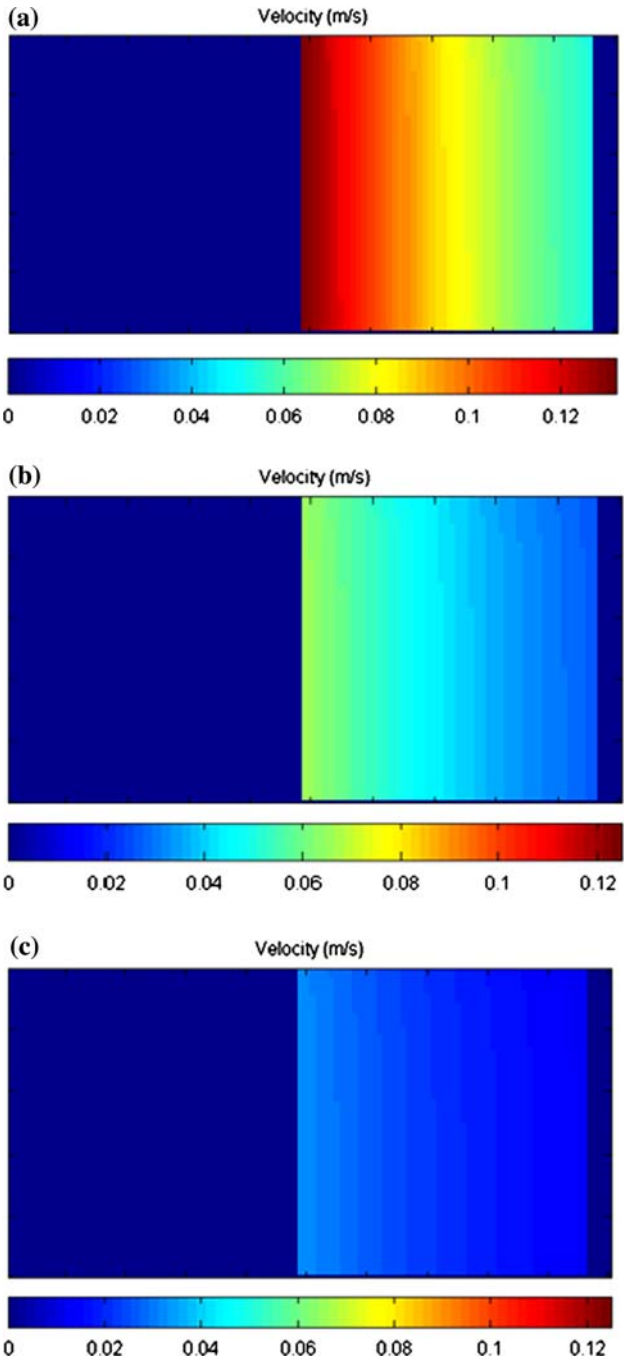

Fig. 9 Velocity field for separate pin effect scenario (FSP at 400 rpm and 0.847 mm/s): (a) Full sticking at the pin/sheet interface (C = 1.0), (b) 50% sticking at the pin/sheet interface (C = 0.5), and (c) 25% sticking at the pin/sheet interface (C = 0.25)

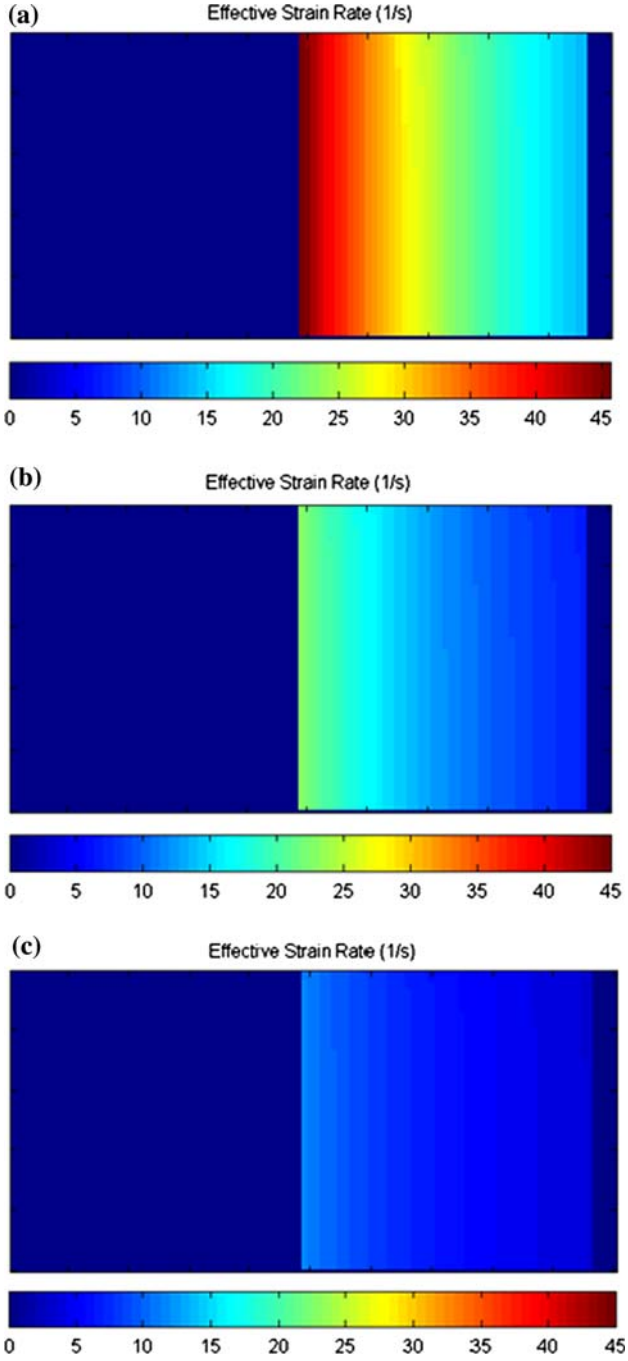

Fig. 10 Strain rate distribution for separate pin effect scenario (FSP at 400 rpm and 0.847 mm/s): (a) full sticking at the pin/sheet interface (C = 1.0), (b) 50% sticking at the pin/sheet interface (C = 0.5), and (c) 25% sticking at the pin/sheet interface (C = 0.25)

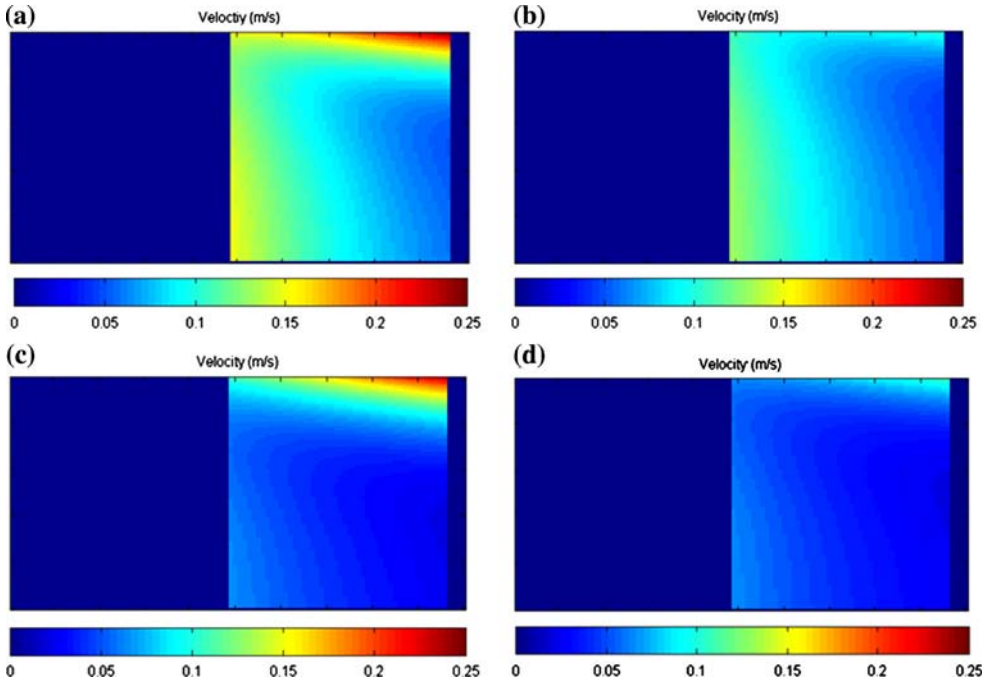

Fig. 11 Velocity field for combined shoulder/pin effect scenario (FSP at 400 rpm and 0.847 mm/s): (a) full sticking at the shoulder/sheet interface (A = 1.0) and full sticking at the pin/sheet interface (C = 1.0), (b) 50% at the shoulder/sheet interface sticking (A = 0.5) and full sticking at the pin/sheet interface (C = 1.0), (c) full sticking at the shoulder/sheet interface (A = 1.0) and 50% sticking at the pin/sheet interface (C = 0.5), and (d) 50% sticking at the shoulder/sheet interface (A = 0.5) and 50% sticking at the pin/sheet interface (C = 0.5)

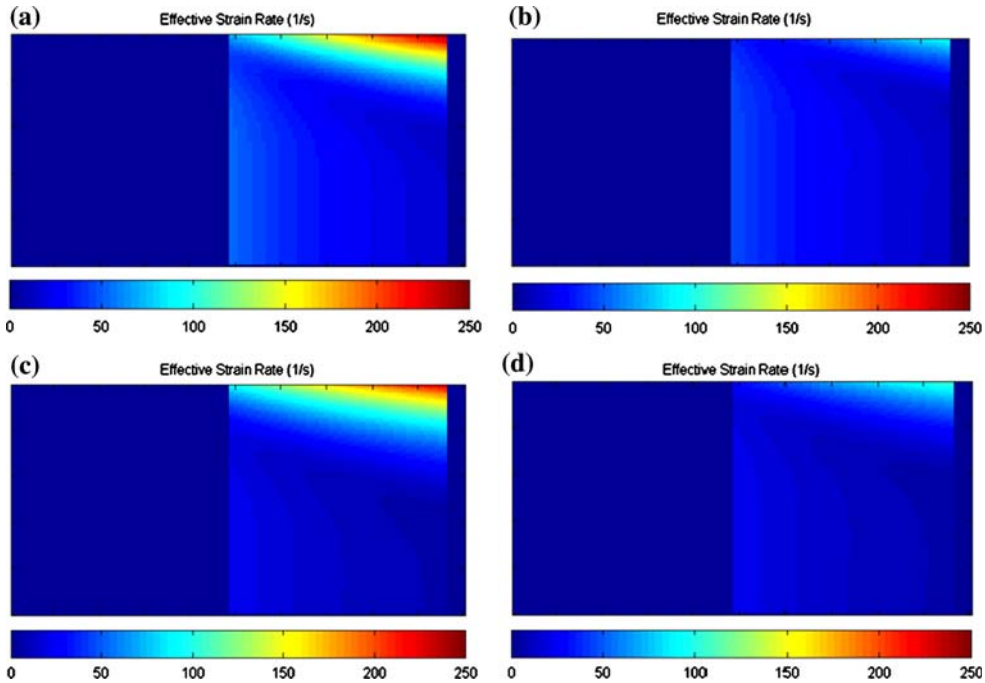

Fig. 12 Strain rate distribution for combined shoulder/pin effects scenario (FSP at 400 rpm and 0.847 mm/s): (a) full sticking at the shoulder/sheet interface (A = 1.0) and full sticking at the pin/sheet interface (C = 1.0), (b) 50% at the shoulder/sheet interface sticking (A = 0.5) and full sticking at the pin/sheet interface (C = 1.0), (c) full sticking at the shoulder/sheet interface (A = 1.0) and 50% sticking at the pin/sheet interface (C = 0.5), and (d) 50% sticking at the shoulder/sheet interface (A = 0.5) and 50% sticking at the pin/sheet interface (C = 0.5)

increase as the rotational speed increases. The effect of the translational speed, however, is negligible, due to the fact that the translational speed is very small compared to the rotational speed. However, this does not mean that the effect of translational speed on the process is negligible. The thermal fields generated during the process were found to be very sensitive to translational as well as rotational speeds (Ref 14). Increasing the rotational speed increases the temperature due to increased heat generation from friction and plastic deformation. On the other hand, increasing the translational speed reduces

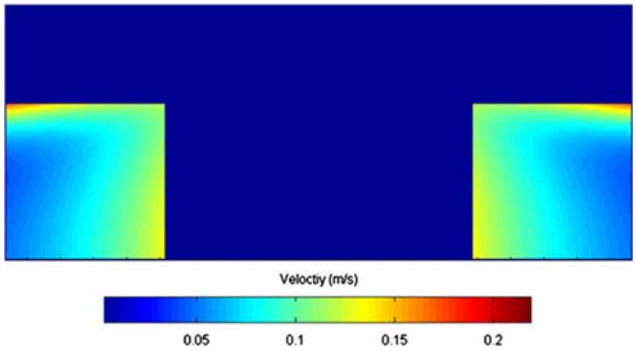

Fig. 13 Predicted shape of the deformation zone (velocity field for FSP at 400 rpm and 0.847 mm/s)

the exposure time of the material to the generated heat and thus reducing the temperature (Ref 14). Therefore, it is very important to choose the optimal process parameters that ensure generation of enough heat to soften the material in order to achieve large plastic flow while limiting excessive heat to prevent significant grain growth. The current model deals only with the mechanical aspect of the process and must be integrated with a thermal model to accurately describe the process. The development of the thermal model using advanced CFD analysis is currently underway.

3.3 Interfacial Contact Conditions

The contact condition at the shoulder/material and pin/material interfaces (whether they are full sticking, full slipping, or partial sticking/slipping) plays a critical role in determining the velocity and strain rate fields. One of the unique features of the proposed model is its ability to accommodate different contact conditions. The contact condition at the interfaces is defined through the constants A and C in the state variables' equations (Eq 1-4). Figure 7 and 8 shows the effect of different contact conditions at the tool/sheet interfaces on the material velocity and strain rate (due to shoulder only). The figures clearly show the ability of the model to capture the actual behavior at different contact conditions. For full sticking, more material flow will result from the shoulder movement when compared to, for example, 50% sticking and 50% slipping. The same results are observed for the effect of contact condition at the pin/material interface on material velocity and strain rate (due to pin only), as illustrated in Fig. 9 and 10. Figure 11 and 12 shows the velocity fields and the strain rate distributions for different combinations of the contact conditions at the two interfaces due to the combined effects of the pin and the shoulder. It is clear that more material flow (more velocity and strain rate) results when the sticking contact conditions exist compared to partial sticking/partial slipping. The results shown in Fig 7-12 can be very useful in designing the tool and selecting the applied pressure in the thickness direction to control the material flow during FSP.

3.4 Validation of Current Results

The preceding paragraphs show that the proposed model is capable of capturing the effects of various process parameters on the material flow during FSP. The shape of the deformation zone is another important piece of information that can be predicted using the proposed model. Figure 13 shows the velocity field in the processed zone. The deformation field is directly related to the velocity field. Hence, one can predict the shape of the deformation fields from the velocity fields. The shape of the deformation field shown in Fig. 13 is in excellent agreement with the shapes of experimentally determined deformation fields reported in the literature [see for example, Ericsson et al. (Ref 16) and Hassan et al. (Ref 17)].

4. Conclusions

The proposed model is capable of predicting the velocity fields and the strain rate distributions within the processed zone of a FS-processed material in terms of the process parameters. The model allows examining the effects of different parameters such as: shoulder and pin, rotational and translational speeds, and different interfacial contact conditions. The obtained velocity and strain rate values are in agreement with reported values in the literature. In addition, the model can successfully capture the shape of the deformation field. The current model deals only with the mechanical aspects of the process and can serve as a first step toward developing a comprehensive model that also includes the thermal aspects of the process. Such a comprehensive model can be used to predict the resulting microstructure during FSP. A thermal model using CFD analysis is currently being developed.

Acknowledgment

The support of the National Science Foundation, CAREER Award # DMI-0238712, is acknowledged.

References

1. W. Thomas, E. Nicholas, J. Needham, M. Murch, P. Temlesmith, and C. Dawes, GB Patent Application No. 9125978.8, December 1991
2. Z. Ma, R. Mishra, and M. Mahoney, Superplastic Deformation Behaviour of Friction Stir Processed 7075Al Alloy, *Acta Mater.*, 2002, **50**, p 4419–4430
3. J. Su, T. Nelson, and C. Sterling, Friction Stir Processing of Large-Area Bulk UFG Aluminum Alloys, *Scripta Mater.*, 2005, **52**, p 135–140
4. M. Khraisheh, B. Darras, P. Kalu, M. Adams-Hughes, and N. Chandra, Correlation Between the Microstructure and Forces Generated During Friction Stir Processing of AA5052, *Mater. Sci. Forum*, 2005, **475-479**, p 3043–3046
5. B. Darras, M. Khraisheh, F. Abu-Farha, and M. Omar, Friction Stir Processing of AZ31 Commercial Magnesium Alloy, *J. Mater. Process. Technol.*, 2007, **191**, p 77–81
6. P. Ulysse, Three-Dimensional Modeling of Friction Stir-Welding Process, *Int. J. Machine Tools Manuf.*, 2002, **42**, p 1549–1557
7. C. Chang, C. Lee, and J. Huang, Relationship Between Grain Size and Zener-Holloman Parameter During Friction Stir Processing in AZ31 Mg Alloys, *Scripta Mater.*, 2004, **51**, p 509–514
8. P. Heurtier, C. Desrayaud, and F. Montheillet, A Thermomechanical Analysis of the Friction Stir Welding Process, *Mater. Sci. Forum*, 2002, **396-402**, p 1537–1542
9. H. Schmidt, J. Hattel, and J. Wert, An Analytical Model for the Heat Generation in Friction Stir Welding, *Modell. Simul. Mater. Sci. Eng.*, 2004, **12**, p 143–157
10. W. Arbegast, Modeling Friction Stir Joining as a Metal Working Process, *Hot Deformation of Aluminum Alloys III*, TMS Annual Meeting, San Diego, CA, 2003, p 313–327

11. J. Schneider and A. Nunes, Thermo-Mechanical Processing in Friction Stir Welds, *Friction Stir Welding and Processing II, Proceedings of a Symposia Sponsered by the Shaping and Forming Committee of the Materials Processing*, TMS Annual Meeting, San Diego, CA, 2003, p 43–51
12. R. Nandan, G. Roy, and T. Debroy, Numerical Simulation of Three-Dimensional Heat Transfer and Plastic Flow During Friction Stir Welding, *Metall. Mater. Trans. A*, 2006, **37A**, p 1247–1259
13. G. Buffa, J. Hua, R. Shivpuri, and L. Fratini, A Continuum Based FEM Model for Friction Stir Welding-Model Development, *Mater. Sci. Eng.*, 2006, **A 419**, p 389–396
14. B. Darras, M. Omar, and M. Khraisheh, Experimental Thermal Analysis of Friction Stir Processing, *Mater. Sci. Forum*, 2007, **539-543**, p 3801–3806
15. L. Malvern, *Introduction to the Mechanics of Continuous Media*, Prentice-Hall, 1969, p 526
16. M. Ericsson, L. Jin, and R. Sandstrom, Fatigue Properties of Friction Stir Overlap Welds, *Int. J. Fatigue*, 2007, **29**, p 57–68
17. Kh. Hassan, A. Norman, D. Price, and P. Pragnell, Stability of Nugget Zone Grain Structures in High Strength Al-Alloy Friction Stir Welds During Solution Treatment, *Acta Mater.*, 2003, **51**, p 1923–1936